Triangle singularities in $\bar{B}^0 \to \chi_{c1} K^- \pi^+$ relevant to $Z_1(4050)$ and $Z_2(4250)$

Satoshi X. Nakamura[1, 2, *]

[1] *University of Science and Technology of China, Hefei 230026, People's Republic of China*
[2] *State Key Laboratory of Particle Detection and Electronics (IHEP-USTC), Hefei 230036, People's Republic of China*

$Z_1(4050)$ and $Z_2(4250)$ observed in $\bar{B}^0 \to \chi_{c1} K^- \pi^+$ by the Belle Collaboration are candidates of charged charmonium-like states that minimally include two quarks and two antiquarks. While $Z_1(4050)$ and $Z_2(4250)$ have been interpreted as tetraquark states previously, we propose a completely different scenario based on a kinematical effect called the triangle singularity. We demonstrate that the triangle singularities cause in the $\chi_{c1}\pi^+$ invariant mass distribution resonance-like bumps that fit very well the Belle data. If these bumps are simulated by the $Z_1(4050)$ and $Z_2(4250)$ resonance excitations, the spin-parity of them are predicted to be 1^- for $Z_1(4050)$ and 1^+ or 1^- for $Z_2(4250)$. The bump corresponding to $Z_1(4050)$ has a highly asymmetric shape, which the Belle data exactly indicate. We show that the asymmetric shape originates from an interplay between the triangle singularity and the opening of the $X(3872)\pi^+$ channel near the triangle-singularity energy. This characteristic lineshape could be used to discriminate different interpretations of $Z_1(4050)$. An interesting prediction from interpreting $Z_1(4050)$ and $Z_2(4250)$ as the triangle singularities is that similar bumps caused by the same mechanisms possibly appear also in $\bar{B}^0 \to J/\psi K^- \pi^+$ data; the already observed $Z_c(4200)$ corresponds to $Z_2(4250)$ of $J^P = 1^+$.

arXiv:1903.08098v3 [hep-ph] 26 Jul 2019

INTRODUCTION

$Z_1(4050)$ and $Z_2(4250)$ ($X(4050)$ and $X(4250)$ in the Particle Data Group (PDG) notation [1]) were observed in the Belle experiment as resonance-like structures in the $\chi_{c1}\pi^+$ invariant mass distribution of $\bar{B}^0 \to \chi_{c1} K^- \pi^+$ [2] [1]. It was not possible to determine the spin(J)-parity(P) of these states. The following analysis in the BaBar experiment [3] did not confirm them because the resonance-like signals were only barely discernible and insignificant. $Z_1(4050)$ and $Z_2(4250)$ are clearly candidates of charged charmonium-like states that minimally include four quarks and thus not belonging to the conventional quark model picture. In order to understand the QCD dynamics and its consequence in the non-perturbative regime, it is highly desirable to establish their existence with higher statistics data in the experimental side, and to clarify their identities such as tetraquark, hadron molecule, or kinematical effect in the theoretical side.

Previous theoretical interpretations of $Z_1(4050)$ and $Z_2(4250)$ are mainly categorized into tetraquark and hadron-molecule. Within the tetraquark picture: (1) a diquark-antidiquark state is [not] assigned to $Z_2(4250)$ [$Z_1(4050)$] [4]; (2) $Z_1(4050)$ is described by a molecular-like tetraquark picture [5]; (3) $Z_1(4050)$ and $Z_2(4250)$ are described with tetraquarks based on a color flux-tube model [6]; (4) $J^{PC} = 0^{++}$ diquark-antidiquark state is not assigned to $Z_1(4050)$ and $Z_2(4250)$ using QCD sum rule (QCDSR) [7]; (5) a tetraquark state is assigned to $Z_2(4250)$ using QCDSR [8]. Meanwhile, within the hadron-molecule picture: (1) meson-exchange models disfavor hadron-molecule pictures for $Z_1(4050)$ and $Z_2(4250)$ [9–11]; (2) $D_1\bar{D}$ molecule state is assigned to $Z_2(4250)$ based on QCDSR [12]. For a more complete summary, see reviews [13, 14].

In this work, we propose a completely different interpretation of $Z_1(4050)$ and $Z_2(4250)$. This is to associate $Z_1(4050)$ and $Z_2(4250)$ with triangle singularities (TS) [15–17], which is a kinematical effect, arising from triangle diagrams depicted in Figs. 1(a) and 1(b) (we refer to them as the triangle diagrams A and B hereafter), respectively. The diagrams consist of experimentally well-established hadrons including $X(3872)$ ($\chi_{c1}(3872)$ in the PDG). The TS can occur only when three particles in the loop go through a classically allowed kinematics (on-shell and collinear in the center-of-mass (CM) frame) at the same time, and can generate a resonance-like spectrum bump; see an illustrative discussion in Ref. [18] for a mathematical detail. Applications of TS to phenomenology have become popular these days [18–30], such as explaining isospin violations in $\eta(1405/1475) \to 3\pi$ [19, 20], and interpreting recently discovered hidden charm pentaquark $P_c(4450)^+$ [18, 21, 22] and $a_1(1420)$ [23, 24].

Recently we also applied TS [31] to interpreting $Z_c(4430)$ [32–34] and $Z_c(4200)$ [35], charged charmonium-like state candidates, observed in $\bar{B}^0 \to \psi(2S) K^- \pi^+$ and $J/\psi K^- \pi^+$. We successfully explained their properties (J^P, mass, width, Argand plot) extracted in the experiments. The presence [absence] of $Z_c(4200)[Z_c(4430)]$-like contribution in $\Lambda_b^0 \to J/\psi p \pi^-$ [36] was also explained in terms of the TS.

The present work shows that $Z_1(4050)$ and $Z_2(4250)$ can also be consistently interpreted as TS, provided the TS have experimentally detectable strengths. We demonstrate that the triangle diagram A [B] creates a $Z_1(4050)$ [$Z_2(4250)$]-like bump in the $\chi_{c1}\pi^+$ invariant mass ($m_{\chi_{c1}\pi}$) distribution of $\bar{B}^0 \to \chi_{c1} K^- \pi^+$. Simulating the bumps with the $Z_1(4050)$ and $Z_2(4250)$ resonance excitations, $J^P = 1^-$ and $1^\pm$ are predicted, respectively.

[1] We implicitly include the charge conjugate mode throughout.

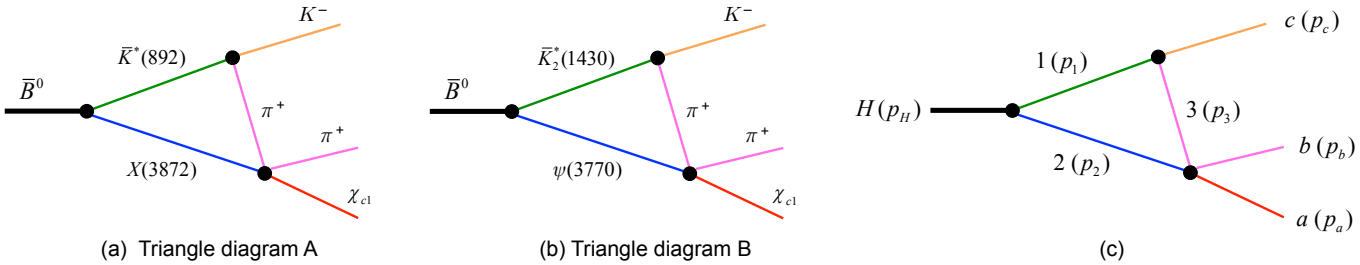


FIG. 1. Triangle diagrams contributing to $\bar{B}^0 \to \chi_{c1}K^-\pi^+$ (a,b). The triangle singularity from the diagram (a) [(b)] generates a $Z_1(4050)$ [$Z_2(4250)$]-like bump in the $\chi_{c1}\pi^+$ invariant mass distribution. A generic triangle diagram (c) defines particle labels and, in the parentheses, their momenta.

The Breit-Wigner masses and widths fitted to the bumps agree very well with those of $Z_1(4050)$ and $Z_1(4250)$ from the Belle analysis [2]. The $Z_1(4050)$-like bump has a highly asymmetric shape as the Belle data exactly indicates. We clarify that the opening of the $X(3872)\pi^+$ channel near the TS energy of $m_{\chi_{c1}\pi} \sim 4.02$ GeV is responsible for it. This characteristic bump shape could discriminate different interpretations of $Z_1(4050)$. We point out that the triangle singularities for $Z_1(4050)$ and $Z_2(4250)$ could also generate similar bumps in $\bar{B}^0 \to J/\psi K^-\pi^+$; the already observed $Z_c(4200)$ corresponds to $Z_2(4250)$ of $J^P = 1^+$.

MODEL

We calculate the $\bar{B}^0 \to \chi_{c1}K^-\pi^+$ decay amplitudes due to the triangle diagrams A and B of Fig. 1. A general formula for the decay amplitude is given by

$$T_{abc,H} = \int d\boldsymbol{p}_1 \, \frac{v_{ab;23}(\boldsymbol{p}_a,\boldsymbol{p}_b;\boldsymbol{p}_2,\boldsymbol{p}_3)\,\Gamma_{3c,1}(\boldsymbol{p}_3,\boldsymbol{p}_c;\boldsymbol{p}_1)}{E - E_2(\boldsymbol{p}_2) - E_3(\boldsymbol{p}_3) - E_c(\boldsymbol{p}_c) + i\epsilon} \times \frac{1}{E - E_1(\boldsymbol{p}_1) - E_2(\boldsymbol{p}_2)} \Gamma_{12,H}(\boldsymbol{p}_1,\boldsymbol{p}_2;\boldsymbol{p}_H) \ , \quad (1)$$

where we have used the particle labels and their momenta in Fig. 1(c). Spin states of the intermediate particles are implicitly summed. The total energy in the CM frame is denoted by E, while the energy of a particle x is $E_x(\boldsymbol{p}_x) = \sqrt{\boldsymbol{p}_x^2 + m_x^2} - i\Gamma_x/2$ with the mass m_x, momentum $\boldsymbol{p}_x$, and width Γ_x; $\Gamma_x \neq 0$ only for unstable intermediate particles 1 and 2. We use the mass and width values of the PDG average [1]. Because $X(3872)$ has a very small width ($\Gamma_{(X(3872)} < 1.2$ MeV), we set it to zero in calculations.

The pion-charmonium interaction is denoted by $v_{ab;23}$ in Eq. (1). The particles 2 is either $X(3872)[J^P = 1^+]$ or $\psi(3770)[1^-]$, the particle a is $\chi_{c1}[1^+]$, and the particles 3 and b are pions$[0^-]$. In calculating the triangle diagram A, we use an s-wave interaction:

$$v^{(\mathrm{A})}_{ab;23}(\boldsymbol{p}_a,\boldsymbol{p}_b;\boldsymbol{p}_2,\boldsymbol{p}_3) = f^{01}_{ab}(p_{ab}) f^{01}_{23}(p_{23})\,\boldsymbol{\epsilon}_a^* \cdot \boldsymbol{\epsilon}_2 \ , \quad (2)$$

where polarization vectors for the particles a and 2 are denoted by $\boldsymbol{\epsilon}_a$ and $\boldsymbol{\epsilon}_2$, respectively. The quantities $f^{01}_{ab}(p_{ab})$ and $f^{01}_{23}(p_{23})$ are form factors that will be defined in Eq. (6); the momentum of the particle i in the ij-CM frame is denoted by $\boldsymbol{p}_{ij}$ and $p_{ij} = |\boldsymbol{p}_{ij}|$. This interaction leaves an s-wave $\chi_{c1}\pi^+$ pair in the final state. Therefore, if a spectrum bump is created by the triangle diagram A in the $m_{\chi_{c1}\pi}$ distribution and is simulated by a resonance-excitation, the resonance has $J^P = 1^-$.

Regarding $v_{ab;23}$ for the triangle diagram B, where the intrinsic parity is different between the incoming and outgoing states, we use

$$v^{(\mathrm{B})}_{ab;23}(\boldsymbol{p}_a,\boldsymbol{p}_b;\boldsymbol{p}_2,\boldsymbol{p}_3) = f^{11}_{ab}(p_{ab}) f^{01}_{23}(p_{23})\,\boldsymbol{\epsilon}_2^* \cdot \boldsymbol{\epsilon}_a \times \boldsymbol{p}_{ab}, \quad (3)$$

which converts s-wave $\psi(3770)\pi^+$ into p-wave $\chi_{c1}\pi^+$. A resonance that simulates a $\chi_{c1}\pi^+$ spectrum bump from the triangle diagram B has $J^P = 1^+$. In Eqs. (2) and (3), the incoming 23-pair is in s-wave and can create a sharp TS bump, being free from the centrifugal barrier. For the triangle diagram B, however, we also examine an interaction of p-wave $\psi(3770)\pi^+$ going to s-wave $\chi_{c1}\pi^+$ because the $\psi(3770)\pi^+$ threshold is rather below the TS energy (~ 4.25 GeV) and the centrifugal barrier would not be so effective. Such an interaction is

$$v^{(\mathrm{B}')}_{ab;23}(\boldsymbol{p}_a,\boldsymbol{p}_b;\boldsymbol{p}_2,\boldsymbol{p}_3) = f^{01}_{ab}(p_{ab}) f^{11}_{23}(p_{23})\,\boldsymbol{\epsilon}_2^* \cdot \boldsymbol{\epsilon}_a \times \boldsymbol{p}_{23}, \quad (4)$$

and the $\chi_{c1}\pi^+$ pair seems to be from a $J^P = 1^-$ resonance.

The $R \to ij$ vertex function, $\Gamma_{ij,R}$ in Eq. (1), is given by

$$\Gamma_{ij,R}(\boldsymbol{p}_i,\boldsymbol{p}_j;\boldsymbol{p}_R) = \sum_{LS} f^{LS}_{ij}(p_{ij})(s_i s_i^z s_j s_j^z | S S^z) \times (LMSS^z | S_R S_R^z) Y_{LM}(\hat{p}_{ij}) \ , \quad (5)$$

with Y_{LM} being spherical harmonics. Clebsch-Gordan coefficients are $(abcd|ef)$ in which the spin of a particle x is denoted by s_x and its z-component s_x^z. We use the form factor $f^{LS}_{ij}(p_{ij})$ in the form of

$$f^{LS}_{ij}(p) = g^{LS}_{ij} \frac{p^L}{\sqrt{E_i(p)E_j(p)}} \left(\frac{\Lambda^2}{\Lambda^2 + p^2}\right)^{2+(L/2)} \ , \quad (6)$$

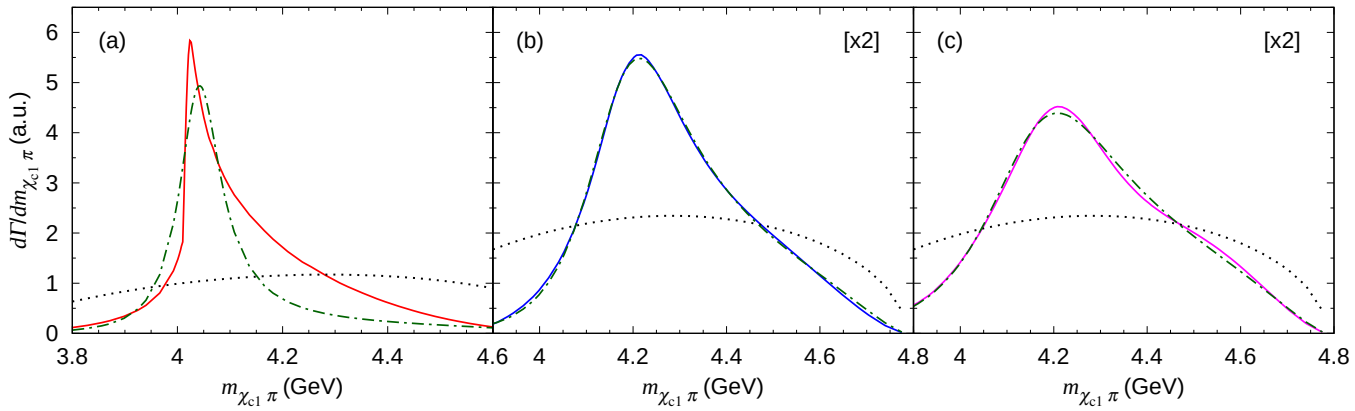


FIG. 2. $\chi_{c1}\pi^+$ invariant mass distributions for $\bar{B}^0 \to \chi_{c1}K^-\pi^+$. The red (blue and magenta) solid curve in the panel (a) [(b) and (c)] is obtained from the triangle diagram A [B]. The interactions $v_{ab;23}$ of Eqs. (2), (3), and (4) are used for (a), (b), and (c), respectively. The green dash-dotted curves are from Breit-Wigner amplitudes fitted to the solid curves. The dotted curves are the phase-space distributions. The solid and dotted curves are normalized to give unity when integrated with respect to $m_{\chi_{c1}\pi}$. The scale for the panels (b) and (c) has been doubled.

which is parametrized with a coupling g_{ij}^{LS} and a cutoff Λ. For the $1 \to 3c$ and $23 \to ab$ interactions, a nonzero value of g_{ij}^{LS} is allowed for only one set of $\{L, S\}$. While the actual values of g_{ij}^{LS} for the $1 \to 3c$ processes can be determined using the $K^*(892)$ and $K_2^*(1430)$ decay widths, experimental and Lattice QCD inputs are currently missing to determine the couplings for the $23 \to ab$ interactions. Experimentally, $X(3872) \to \chi_{c1}\pi^+\pi^-$ has not yet been seen [37], perhaps because $X(3872)$ has a very small width and the phase-space for this final state is small; $\psi(3770) \to \chi_{c1}\pi\pi$ is not kinematically allowed. Here we assume that these couplings are strong enough and set them arbitrary.

Regarding the weak vertices for the $H \to 12$ decays, $g_{ij}^{LS} \neq 0$ is allowed for several sets of $\{L, S\}$ but their values are currently difficult to estimate due to the lack of data. However, the details of these vertices would not be crucial in this work because the main conclusions are essentially determined by the kinematical effects once the structure of $v_{ab;23}$ is fixed as Eqs. (2)-(4). Thus we assume simple structures and detectable strengths. We set $g_{ij}^{LS} \neq 0$ only for $S = |s_1 - s_2|$ (exception: $S = 2$ when using Eq. (4)) and the lowest allowed L; $g_{ij}^{LS} = 0$ for the other $\{L, S\}$. We use the cutoff $\Lambda = 1$ GeV in Eq. (6) throughout unless otherwise stated.

The interactions of Eqs. (2)-(5), evaluated in the CM frame of the two-body subsystem, are further multiplied by kinematical factors to account for the Lorentz transformation to the total three-body CM frame; see Appendix C of Ref. [38]. The Dalitz plot distribution for $H \to abc$ is calculated with $T_{abc,H}$ of Eq. (1) following the procedure detailed in Appendix B of Ref. [38].

RESULTS

In Fig. 2, we present the $\chi_{c1}\pi^+$ invariant mass distributions for $\bar{B}^0 \to \chi_{c1}K^-\pi^+$. The triangle diagram A [B] gives the red [blue and magenta] solid curve in Fig. 2(a) [2(b) and 2(c)]. We also show the phase-space distributions (black dotted curves). The triangle singularity creates clear resonance-like peaks at $m_{\chi_{c1}\pi} \sim 4.02$ GeV in panel (a) and $m_{\chi_{c1}\pi} \sim 4.22$ GeV in panels (b) and (c). It is interesting to observe in Fig. 2(a) that the bump has a significantly asymmetric shape.

We examine how the spectrum shapes shown in Fig. 2 depend on the cutoff Λ of the form factor in Eq. (6). In

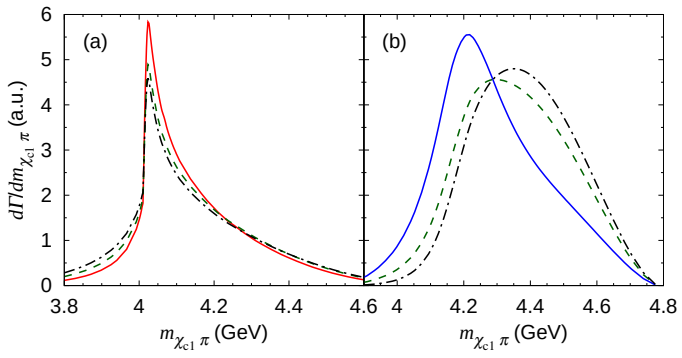


FIG. 3. Cutoff (Λ) dependence of the spectrum shapes generated by triangle diagrams. The panels (a) and (b) correspond to the triangle diagrams A and B, respectively. The red and blue solid curves are the same as those in Fig. 2(a) and 2(b), respectively, where $\Lambda = 1$ GeV. The green dashed, and black dash-dotted curves are obtained with $\Lambda = 1.5$, and 2 GeV, respectively. All the curves are normalized as in Fig. 2.

Fig. 3, the spectrum shapes calculated with $\Lambda = 1$, 1.5, and 2 GeV are shown. The resonance-like peak structures due to the kinematical singularities are clearly stable over the reasonable cutoff range. In particular, the peak positions of the spectra from the triangle diagram A are, as in Fig. 3(a), almost the same; the width is somewhat broadened as Λ increases. The peak position and width of the spectrum from the triangle diagram B are more dependent on Λ. This would be related to the fact that the unstable particles in the triangle diagram B have wider widths than those in the triangle diagram A, thereby pushing the exact TS further away from the physical region.

Now we simulate the spectra using the conventional resonance-excitation mechanisms, and determine the masses and widths of the fake resonances. The Dalitz plot distributions from the triangle diagrams A and B are fitted with the mechanism of $\bar{B}^0 \to ZK^-$ followed by $Z \to \chi_{c1}\pi^+$. The Breit-Wigner form of Ref. [33] is used for the Z propagation. This Z-excitation mechanism includes fitting parameters such as the Breit-Wigner mass, width, and also the cutoff in Eq. (6) that describes the vertices. The kinematical region included in the fit covers the Dalitz plot distribution larger than 10% of the peak height. The obtained fits are shown by the green dash-dotted curves in Fig. 2. The highly asymmetric bump, the red solid curve in Fig. 2(a), is not well fitted with the Breit-Wigner form, while the bumps in Figs. 2(b) and 2(c) are reasonably fitted. We generate the Dalitz plot distributions for $\Lambda = 1, 1.5$, and 2 GeV as in Fig. 3, fit them as described above, and present the resulting ranges of the Breit-Wigner parameters in Table I along with those of $Z_1(4050)$ and $Z_2(4250)$ from the Belle analysis [2]. The agreement is quite good for $Z_1(4050)$. Meanwhile, the $Z_2(4250)$ mass and width from the Belle analysis have rather large errors, and thus our results for both $J^P = 1^\pm$ assignments easily agree with them.

Let us superimpose the spectra from the triangle diagrams A and B on the Belle data (Fig. 14 of Ref. [2]) as shown in Fig. 4. Although this is a qualitative comparison where any interferences among different mechanisms are not taken into account, the spectrum bumps from the triangle diagrams capture characteristic features of the data. In particular, the asymmetric shape from the triangle diagram A, which has a very sharp rise and a moderate fall-off, is exactly what the data show. In the Belle analysis [2] where the Breit-Wigner form was used to simulate this bump, their model does not seem to fit this sharp peak of the data very well, as seen in Fig. 14 of the reference, perhaps because the Breit-Wigner shape is not what the data call for. As seen in Fig. 2(a), the spectrum shape from the triangle diagram A is significantly different from the Breit-Wigner.

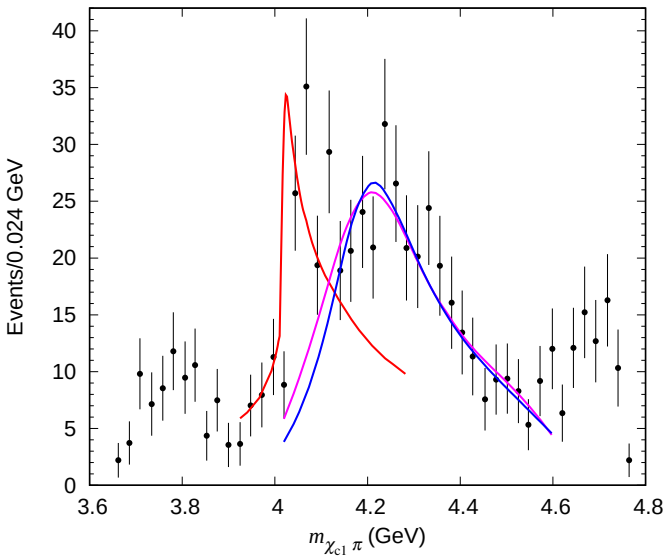


FIG. 4. $\chi_{c1}\pi^+$ invariant mass distributions for $\bar{B}^0 \to \chi_{c1}K^-\pi^+$. The red, blue, and magenta solid curves in Figs. 2(a-c) are modified to include only the contributions in 1.0 GeV^2 $< m^2_{K^-\pi^+} <$ 1.75 GeV^2, and superimposed on the Belle data (Fig. 14 of Ref. [2]) from the same kinematical constraint. Each of the curves is multiplied by a constant factor and an incoherent constant background is added to fit the data.

TABLE I. Spin-parity J^P (third row), Breit-Wigner mass in MeV (fourth row), and width in MeV (fifth row) for $Z_1(4050)$ and $Z_2(4250)$. The Breit-Wigner parameters for $Z_1(4050)$ [$Z_2(4250)$] are extracted by fitting the Dalitz plot distributions for $\bar{B}^0 \to \chi_{c1}K^-\pi^+$ generated by triangle diagram of Fig. 1(a) [1(b)]. The parameter ranges are from the cutoff dependence. The parameters from the Belle analysis [2] are also shown; the first (second) errors are statistical (systematic).

$Z_1(4050)$		$Z_2(4250)$		
Fig. 1(a)	Belle [2]	Fig. 1(b)		Belle [2]
1^-	$?^?$	1^+	1^-	$?^?$
4041 ± 1	$4051 \pm 14^{+20}_{-41}$	4247 ± 53	4309 ± 116	$4248^{+44+180}_{-29-35}$
115 ± 17	82^{+21+47}_{-17-22}	345 ± 67	468 ± 90	$177^{+54+316}_{-39-61}$

It would be worthwhile to address how this peculiar asymmetric shape comes about from the triangle diagram A. By closely observing the spectrum shown in Fig. 2(a) or an enlarged one shown by the red solid curve in Fig. 5, the sharp rise of the spectrum starts from an abrupt bend at $m_{\chi_{c1}\pi} \sim 4.01$ GeV where the $X(3872)\pi^+$ channel opens. This implies that the sharp rise is assisted by the opening of the $X(3872)\pi^+$ channel. We indeed confirm this idea, as shown by the black dash-two-dotted curve in Fig. 5, by turning off the on-shell $X(3872)\pi^+$ contribution arising from $+i\epsilon$ in the denominator of Eq. (1).

The proximity of the $X(3872)\pi^+$ threshold to the TS energy ($\sim$ 4.025 GeV) is also important to create the large asymmetry. To see this, we change the $X(3872)$ and

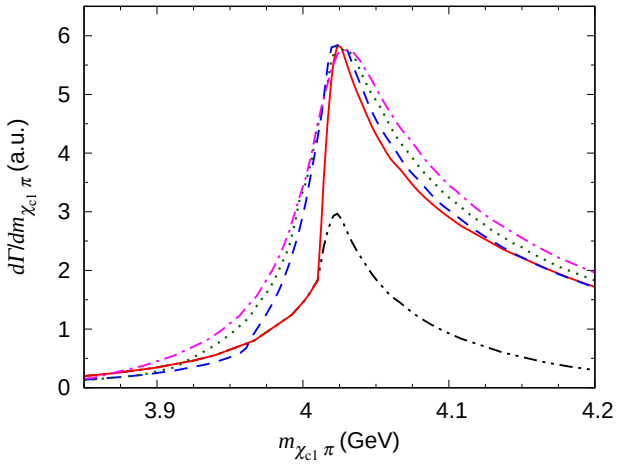


FIG. 5. $\chi_{c1}\pi^+$ invariant mass distributions for $\bar{B}^0 \to \chi_{c1}K^-\pi^+$ calculated with the triangle diagram A. The red solid, blue dashed, green dotted, and magenta dash-dotted curves are calculated using the $X(3872)\pi^+$ threshold energy smaller than the PDG value by 0, 50, 100, and 150 MeV, respectively; see the text for details. All these curves, being scaled, have the same peak height. The black dash-two-dotted curve is obtained from the red solid one by turning off the on-shell $X(3872)\pi^+$ contribution.

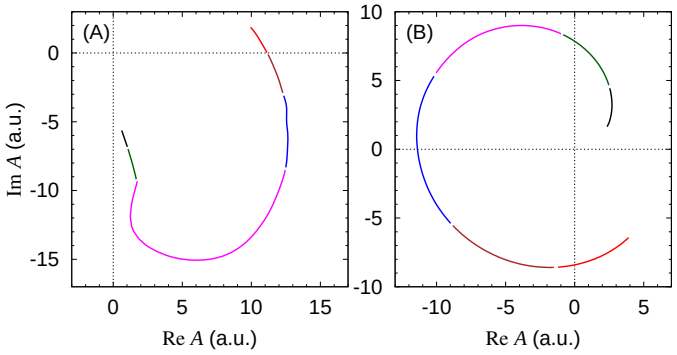


FIG. 6. Argand plots from the triangle diagrams A (left) and B (right), corresponding to the spectra of Fig. 2(a) and 2(b), respectively. Six curved segments belong to six bins equally-separating the range of $M_{BW}-\Gamma_{BW} \le m_{\chi_{c1}\pi} \le M_{BW}+\Gamma_{BW}$; M_{BW} = 4042 (4194) MeV and Γ_{BW} = 97 (278) MeV for triangle diagram A (B). $m_{\chi_{c1}\pi}$ increases counterclockwise.

$K^*(892)$ masses to lower the $X(3872)\pi^+$ threshold while keeping the spectrum peak position almost the same. We use, in unit of MeV, $(m_{X(3872)}, m_{K^*(892)})$=(3822, 1084), (3772, 1218), and (3722, 1330) to lower the threshold by 50, 100, and 150 MeV, respectively. The spectra calculated with these altered masses, presented in Fig. 5, show that the rise of the bump becomes significantly more moderate as the threshold is lowered. In this way, the $Z_1(4050)$-bump shape observed in the Belle data is explained with well-founded physics, TS and the channel opening near the TS energy, included in the triangle diagram A.

The asymmetric $Z_1(4050)$-bump shape could sensitively discriminate different interpretations of $Z_1(4050)$. A compelling model should explain not only the mass, width, and J^P of $Z_1(4050)$, but also its characteristic spectrum shape. So far, only our model has successfully addressed this question. It is also highly desirable to establish the spectrum shape with higher statistics data, considering that the Belle data still have large error bars.

It would be interesting to discuss the possibility of finding $Z_1(4050)$ and $Z_2(4250)$-like bumps in other processes. We point out that, actually, the $Z_2(4250)(J^P = 1^+)$-like bump in $\bar{B}^0 \to \chi_{c1}K^-\pi^+$ and the $Z_c(4200)$-like bump in $\bar{B}^0 \to J/\psi K^-\pi^+$ [35, 39] can be created by the same TS [31] from the triangle diagram B and thus are very similar. Meanwhile, if the $Z_1(4050)$-like bump in the $\bar{B}^0 \to \chi_{c1}K^-\pi^+$ data is generated by the triangle diagram A, the same diagram but χ_{c1} replaced by J/ψ should contribute to $\bar{B}^0 \to J/\psi K^-\pi^+$ because the $X(3872) \to J/\psi\pi^+\pi^-$ coupling is known to exist. We calculated the $Z_1(4050)$-like spectrum for $\bar{B}^0 \to J/\psi K^-\pi^+$ using the modified triangle diagram A; the pion-charmonium interaction is now given by Eq. (3). The spectrum looks almost the same as the red solid curve of Fig. 2(a). While a $Z_1(4050)$-like bump has not yet been observed in $\bar{B}^0 \to J/\psi K^-\pi^+$ [35, 39], the quality of the current data still leaves a possibility of finding it in the $J/\psi\pi^+$ spectrum data of higher statistics. Although the possibility certainly depends on competitions with other mechanisms, this is an interesting prediction from the TS-based interpretation of the $Z_1(4050)$ bump.

Finally, we present Argand plots from the triangle diagrams A and B; we use Eq. (3) for the diagram B. Because Z_1 (Z_2) and K^- are relatively in p-wave, the angle-independent part of the amplitude is:

$$A(m_{ab}^2) = \int d\Omega_{p_c} d\Omega_{p_{ab}} Y^*_{1,-s^z_{\chi_{c1}}}(\hat{p}_c) Y^*_{\ell 0}(\hat{p}_{ab}) M_{abc,H} \quad (7)$$

with $\ell = 0$ and 1 for the diagrams A and B, respectively; $s^z_{\chi_{c1}}$ is the z-component of the χ_{c1} spin and m_{ab} the ab invariant mass. See Eq. (B3) of Ref. [38] for the relation between the invariant amplitude $M_{abc,H}$ and $T_{abc,H}$ of Eq. (1). $A(m_{ab}^2)$ is shown in Fig. 6 as Argand plots. Both the triangle diagrams A and B create counterclockwise behaviors, seemingly similar to resonances.

CONCLUSION

We demonstrated that triangle singularities (TS) from the triangle diagrams of Figs. 1(a) and 1(b) cause the bumps in the $\chi_{c1}\pi^+$ invariant mass distribution of $\bar{B}^0 \to \chi_{c1}K^-\pi^+$, and that their positions and shapes, and thus Breit-Wigner parameters fitted to the bumps, agree very well with those found and named as $Z_1(4050)$

and $Z_2(4250)$ in the Belle experiment [2]. Within the resonance-based simulation of these bumps, $J^P = 1^-$ is predicted for $Z_1(4050)$ and $J^P = 1^+$ or 1^- for $Z_2(4250)$. The highly asymmetric shape of $Z_1(4050)$-like bump found by the Belle is well reproduced by our model; the opening of the $X(3872)\pi^+$ channel near the TS energy causes the abrupt increase of the spectrum. This characteristic lineshape, which could discriminate different interpretations of $Z_1(4050)$, is yet to be accounted for by any other hadron structure models. We also discussed the possibility of finding bumps, caused by the same TS for $Z_1(4050)$ and $Z_2(4250)$, in $\bar{B}^0 \to J/\psi K^-\pi^+$; $Z_c(4200)$ found in $\bar{B}^0 \to J/\psi K^-\pi^+$ can be identified with $Z_2(4250)$ of $J^P = 1^+$. The kinematic effects, TS and the channel opening, essentially determine the shape and position of the spectrum bumps, once the spin-parity of the $\chi_{c1}\pi^+$ system is specified by Eqs. (2)-(4); the uncertainty of the remaining dynamical details would not largely change the presented results.

This work is in part supported by National Natural Science Foundation of China (NSFC) under contracts 11625523.

* satoshi@ustc.edu.cn

[1] M. Tanabashi et al. (Particle Data Group), Phys. Rev. D **98**, 030001 (2018).
[2] R. Mizuk et al. (Belle Collaboration), Phys. Rev. D **78**, 072004 (2008).
[3] J.P. Lees et al. (BaBar Collaboration), Phys. Rev. D **85**, 052003 (2012).
[4] D. Ebert, R.N. Faustov, and V.O. Galkin, Eur. Phys. J. C **58**, 399 (2008).
[5] S. Patel, M. Shah, and P.C. Vinodkumar, Eur. Phys. J. A **50**, 131 (2014).
[6] C. Deng, J. Ping, H. Huang, and F. Wang, Phys. Rev. D **92**, 034027 (2015).
[7] Z.-G. Wang, Commun. Theor. Phys. **63**, 466 (2015).
[8] Z.-G. Wang, Eur. Phys. J. C **62**, 375 (2009).
[9] X. Liu, Z.-G. Luo, Y.-R. Liu, and S.-L. Zhu, Eur. Phys. J. C **61**, 411 (2009).
[10] Y.-R. Liu and Z.-Y. Zhang, Phys. Rev. C **80**, 015208 (2009).
[11] G.-J. Ding, Phys. Rev. D **79**, 014001 (2009).
[12] S.H. Lee, K. Morita, and M. Nielsen, Phys. Rev. D **78**, 076001 (2008).
[13] H.-X. Chen, W. Chen, X. Liu, and S.-L. Zhu, Phys. Rep. **639**, 1 (2016).
[14] R.M. Albuquerque, J.M. Dias, K.P. Khemchandani, A. Martinez Torres, F.S. Navarra, M. Nielsen, and C.M. Zanetti, arXiv:1812.08207 [hep-ph].
[15] L.D. Landau, Nucl. Phys. **13**, 181 (1959).
[16] S. Coleman and R.E. Norton, Nuovo Cim. **38**, 438 (1965).
[17] R. J. Eden, P. V. Landshoff, D. I. Olive and J. C. Polkinghorne, The Analytic S-Matrix, (Cambridge University Press, Cambridge, England, 1966).
[18] M. Bayar, F. Aceti, F.-K. Guo, and E. Oset, Phys. Rev. D **94**, 074039 (2016).
[19] J.-J. Wu, X.-H. Liu, Q. Zhao, and B.-S. Zou, Phys. Rev. Lett. **108**, 081803 (2012).
[20] F. Aceti, W.H. Liang, E. Oset, J.J. Wu, and B.S. Zou, Phys.Rev. D **86**, 114007 (2012).
[21] F.-K. Guo, U.-G. Meißner, W. Wang, and Z. Yang, Phys. Rev. D **92**, 071502 (2015).
[22] X.-H. Liu, Q. Wang, and Q. Zhao, Phys. Lett. **B757**, 231 (2016).
[23] M. Mikhasenko, B. Ketzer, and A. Sarantsev, Phys. Rev. D **91**, 094015 (2015).
[24] F. Aceti, L.R. Dai, and E. Oset, Phys. Rev. D **94**, 096015 (2016).
[25] S. Sakai, E. Oset and W.H. Liang, Phys. Rev. D **96**, 074025 (2017).
[26] X.H. Liu and U.-G. Meißner, Eur. Phys. J. C **77**, 816 (2017).
[27] S. Sakai, E. Oset and A. Ramos, Eur. Phys. J. A **54**, 10 (2018).
[28] L.R. Dai, R. Pavao, S. Sakai and E. Oset, Phys. Rev. D **97**, 116004 (2018).
[29] Z. Cao and Q. Zhao, Phys. Rev. D **99**, 014016 (2019).
[30] J.J. Xie and F.K. Guo, Phys. Lett. B **774**, 108 (2017).
[31] S.X. Nakamura and K. Tsushima, arXiv:1901.07385.
[32] S.K. Choi et al. (Belle Collaboration), Phys. Rev. Lett. **100**, 142001 (2008).
[33] K. Chilikin et al. (Belle Collaboration), Phys. Rev. D **88**, 074026 (2013).
[34] R. Aaij et al. (LHCb Collaboration), Phys. Rev. Lett. **112**, 222002 (2014).
[35] K. Chilikin et al. (Belle Collaboration), Phys. Rev. D **90**, 112009 (2014).
[36] R. Aaij et al. (LHCb Collaboration), Phys. Rev. Lett. **117**, 082003 (2016).
[37] V. Bhardwaj et al. (Belle Collaboration), Phys. Rev. D **93**, 052016 (2016).
[38] H. Kamano, S.X. Nakamura, T.-S.H. Lee, and T. Sato, Phys. Rev. D **84**, 114019 (2011).
[39] R. Aaij et al. (LHCb collaboration), Phys. Rev. Lett. **122**, 152002 (2019).